LETTERS

Deletion of vascular endothelial growth factor in myeloid cells accelerates tumorigenesis

Christian Stockmann[1], Andrew Doedens[1], Alexander Weidemann[1], Na Zhang[1], Norihiko Takeda[1], Joshua I. Greenberg[2], David A. Cheresh[3] & Randall S. Johnson[1]

Angiogenesis and the development of a vascular network are required for tumour progression, and they involve the release of angiogenic factors, including vascular endothelial growth factor (VEGF-A), from both malignant and stromal cell types[1]. Infiltration by cells of the myeloid lineage is a hallmark of many tumours, and in many cases the macrophages in these infiltrates express VEGF-A[2]. Here we show that the deletion of inflammatory-cell-derived VEGF-A attenuates the formation of a typical high-density vessel network, thus blocking the angiogenic switch in solid tumours in mice. Vasculature in tumours lacking myeloid-cell-derived VEGF-A was less tortuous, with increased pericyte coverage and decreased vessel length, indicating vascular normalization. In addition, loss of myeloid-derived VEGF-A decreases the phosphorylation of VEGF receptor 2 (VEGFR2) in tumours, even though overall VEGF-A levels in the tumours are unaffected. However, deletion of myeloid-cell VEGF-A resulted in an accelerated tumour progression in multiple subcutaneous isograft models and an autochthonous transgenic model of mammary tumorigenesis, with less overall tumour cell death and decreased tumour hypoxia. Furthermore, loss of myeloid-cell VEGF-A increased the susceptibility of tumours to chemotherapeutic cytotoxicity. This shows that myeloid-derived VEGF-A is essential for the tumorigenic alteration of vasculature and signalling to VEGFR2, and that these changes act to retard, not promote, tumour progression.

To test the role of myeloid-cell-derived VEGF in tumour progression, we created an *in vivo*, cell-lineage-specific, targeted deletion of *Vegfa* by means of crosses of the *loxP*-flanked *Vegfa* allele[3] to the lysozyme M promoter-driven Cre recombinase[4]; this expression is specific to cells of the myeloid lineage, including neutrophils and macrophages, but not dendritic cells (*LysMCre*/*VEGF*+^{f}/+^{f})[4]. This results in *Vegfa* gene excision in about 75% of isolated neutrophils, peritoneal macrophages[5] and tumour-associated macrophages (Supplementary Fig. 1a).

To determine the function of myeloid-cell-derived VEGF-A in an autochthonous mouse model of breast cancer, we then crossed these alleles to the MMTV-*PyMT* transgenic mouse strain[6]. To mitigate the influence of strain variation, individual transgenic alleles were backcrossed to a more than 99% C57Bl/6J strain background (as assayed by single-nucleotide-polymorphism analysis).

Because both genotypes carry the *PyMT* transgene, mice with a myeloid cell-specific deletion of *Vegfa* (MMTV-*PyMT*/*LysMCre*+/*VEGF*+^{f}/+^{f}) will be termed mutant mice, whereas Cre-negative mice (MMTV-*PyMT*/*LysMCre*−/*VEGF*+^{f}/+^{f}) will be termed wild-type (WT) mice (Supplementary Fig. 1b).

To determine the time point of tumour onset, mammary glands of virgin WT and mutant mice were palpated once a week. The first palpable tumour occurred at an average age of 11 weeks (Supplementary Fig. 1d). Tumours were removed at two different time points, and the total tumour burden for each mouse was evaluated. At 16 weeks, tumours from WT and mutant animals showed no difference in total tumour mass (Supplementary Fig. 1e). However, at 20 weeks, mutant mice had a significantly higher tumour burden than their WT littermates (Fig. 1a). At this point, tumours from WT animals had increased their total mass by almost 400% relative to the 16-week time point; tumours from mutants showed an increase in tumour mass of almost 600% in comparison with the 16-week time point.

A quantitative analysis of proliferating cells showed that the number of cells staining positive for proliferating-cell nuclear antigen (PCNA) increased with progression to malignancy (Supplementary Fig. 1h) and that loss of myeloid-cell-derived VEGF-A increased proliferation rates significantly in the early stages of malignant transformation (Supplementary Fig. 1h). Immunohistological detection of polyoma middle T antigen and PCNA showed that the proliferating cell types were primarily mammary epithelium (Supplementary Fig. 1f).

To address the question of whether the level of malignant progression mirrored tumour mass results, we assessed tumour progression histologically for each time point on the basis of representative sections from each mammary gland by using the criteria described previously[7], in a blinded fashion. As depicted in Fig. 1b, at the time point of 16 weeks, most mammary gland tissues from both WT and mutant animals were still at premalignant stages (96.2% and 89.5%, by area, respectively). After 20 weeks, most tissues in mutant mice had progressed to malignant stages (early carcinoma 38.0%; late carcinoma 52.5%). In WT animals, mammary tissues were primarily at premalignant (30.9%) and early carcinoma (50.2%) stages; a minority of the tissue (18.9%) possessed late-carcinomatous lesions (Fig. 1b). These results indicated that tumours develop more rapidly in the absence of macrophage-derived VEGF-A.

Quantitative analysis of vessel density was then performed (Fig. 1c–e and Supplementary Fig. 1g). In WT mice, premalignant lesions have a low vascular density, which is decreased in mutant mice lacking myeloid VEGF-A (Fig. 1c). Increased vascular density was found in tumours that had progressed to the malignant, early carcinoma stage, which is consistent with the occurrence of an 'angiogenic switch' during the transition to malignancy (Fig. 1c). In late-carcinoma-stage tumours formed by multiple solid nodular areas, the overall vascular density was similar to that seen in the early carcinoma stage in WT animals. However, in mutant mice, the malignancy-associated increased vascularization seen in WT animals did not occur (Fig. 1c). The length and the tortuosity of tumour blood vessels were also affected by the mutation: as depicted in Fig. 1d, the average vessel length in tumours in WT mice increased as tumours progressed to malignancy, indicating that vessel elongation has a key function in the formation of a tumour vessel network in

[1]Molecular Biology Section, Division of Biological Sciences, [2]Department of Surgery, and [3]Department of Pathology and Moores Cancer Center, University of California, San Diego, San Diego, California 92093, USA.

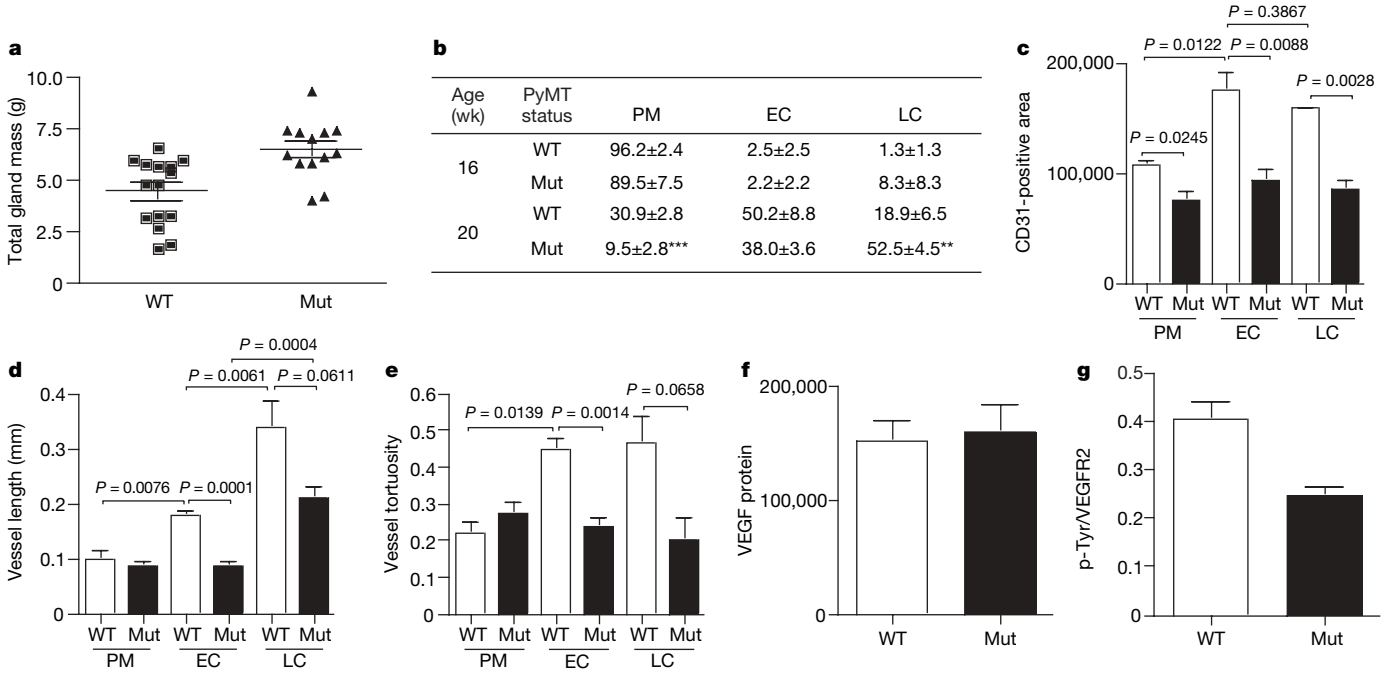

Age (wk)	PyMT status	PM	EC	LC
16	WT	96.2±2.4	2.5±2.5	1.3±1.3
	Mut	89.5±7.5	2.2±2.2	8.3±8.3
20	WT	30.9±2.8	50.2±8.8	18.9±6.5
	Mut	9.5±2.8***	38.0±3.6	52.5±4.5**

Figure 1 | Deletion of VEGF in myeloid cells results in reduced vascularization but accelerated progression of mammary tumours. a, Total tumour mass of PyMT-WT mice ($n = 15$) and PyMT-mutant mice ($n = 13$) at the age of 20 weeks. $P = 0.0018$.The horizontal lines show mean values. **b**, Distribution of PyMT mammary tumours at prototypical premalignant (PM) lesions, malignant early carcinoma (EC) and late carcinoma (LC) stages in percentages (means ± s.e.m.) between genotypes and at the age of 16 weeks ($n = 4$) and 20 weeks (PyMT-WT $n = 4$, PyMT-mutant $n = 9$). Two asterisks, $P < 0.01$; three asterisks, $P < 0.001$. **c**, Quantitative analysis of the area in pixels covered by CD31-positive cells within a tumour section for each stage ($n = 4$). **d**, Development of vessel length in PyMT-tumours during malignant progression as determined by tracing CD31-positive vessels that were exposed in a longitudinal cut ($n = 4$). **e**, Analysis of vessel tortuosity based on CD31-stained tumour sections ($n = 4$). **f**, Quantitative analysis by photon emission of the VEGF signal (PyMT-WT $n = 7$, PyMT-mutant $n = 4$). $P = 0.7678$. **g**, Ratio of phosphotyrosine (p-Tyr) and VEGFR2 signal intensities as a measure of receptor activation (PyMT-WT $n = 7$, PyMT-mutant $n = 4$). $P = 0.0102$. Error bars show s.e.m.

this model. Along with this increase, blood vessel tortuosity more than doubled in malignant lesions in WT mice (Fig. 1e). In tumours within mutant mice, there was no increase in vessel length before the late carcinoma stage (Fig. 1d), and vessel tortuosity never changed in the mutants (Fig. 1e).

Gene-expression analysis of lysates of mammary tumours from mice at the endpoint age of 20 weeks did not reveal any increase in expression of hypoxia markers, such as *Pgk1*, encoding phosphoglycerate kinase 1 (Supplementary Fig. 1i). However, this analysis of tumours did demonstrate that there was higher expression of *Vegfa* messenger RNA in tumours from mutant animals (Supplementary Fig. 1j). This was not mirrored by changes in VEGF-A protein, however, which did not vary in tumour lysates from WT and mutant animals (Fig. 1f).

We next wished to determine whether signalling to the tumour endothelium was affected by the loss of myeloid-derived VEGF-A. VEGFR2 is a primary endothelial cell-specific receptor tyrosine kinase that participates in VEGF signalling. By immunoprecipitating VEGFR2 from tumour lysates and probing with anti-phosphotyrosine followed by anti-VEGFR2 antibody by means of western blotting, we were able to quantify activated and total VEGFR2 from WT and mutant tumours. As shown in Fig. 1g, loss of myeloid-derived VEGF-A causes a roughly 50% decrease in the ratio of phosphorylated VEGFR2 to total VEGFR2 in comparison with WT tumour lysates. Decreased VEGFR2 phosphorylation suggests that myeloid-cell-derived VEGF-A has a unique function in tumour vascularization that cannot be compensated for by VEGF-A from other sources within the tumour.

To analyse these effects in fully transformed cells, we next performed experiments with subcutaneous isografts of Lewis lung carcinoma (LLC) cells. LLC tumours in mutant mice lacking myeloid VEGF had significantly greater tumour volumes at day 12 (Fig. 2a), with no genotype-specific differences in tumour infiltration (Supplementary Fig. 2). Flow cytometric analysis demonstrated that macrophages were the predominant myeloid infiltrate and that levels of infiltrating macrophages and less abundant neutrophils were similar across genotypes (Supplementary Fig. 2).

A significant decrease in vascular density and vessel tortuosity was again observed in mutant mice (Fig. 2b, c). An analysis of VEGF-A protein and *Vegfa* mRNA (Supplementary Fig. 3a, b) showed no significant differences between genotypes. However, when VEGFR2, phosphorylated VEGFR2 and the ratio of phosphorylated VEGFR2 to total VEGFR2 were quantified (Fig. 2d), activation of VEGFR2 was once again decreased by about 50% in mutant tumours relative to WT tumours.

We next wished to determine the relationship between the expression of myeloid cell VEGF and vessel normalization; to assay this, we immunohistologically detected pericyte coverage of tumour vessels and assayed the levels of pericyte coverage in the tumours (Fig. 2e). As shown, the loss of VEGF-A expression in the myeloid cells resulted in a marked increase in the level of vessel pericyte association, indicating that VEGF-A expression from infiltrating myeloid cells is essential for intratumoral loss of vessel pericyte coverage. Vessel permeability also decreased in tumours from mutant animals (Fig. 2f).

Hypoxia is associated with the growth of solid tumours and with tumorigenic vasculature. We found that the more slowly growing WT tumours had higher levels of hypoxia (Fig. 3a and Supplementary Fig. 3c) and that this occurred even in areas that were extensively vascularized (Supplementary Fig. 3c). Staining of tumour sections for VEGF and F4/80, a macrophage marker, demonstrates that intense VEGF-A immunostaining in WT tumours occurs in regions of high infiltration, whereas in mutant tumours VEGF-A staining is only found outside of infiltrated regions (Supplementary Fig. 3d); this shows how VEGF-A from myeloid cells could have an acute and localized effect on tumour vasculature.

To determine whether the vascular changes we describe confer an increased susceptibility to cytotoxic agents, we administered the chemotherapy agent cyclophosphamide to WT and mutant LLC-

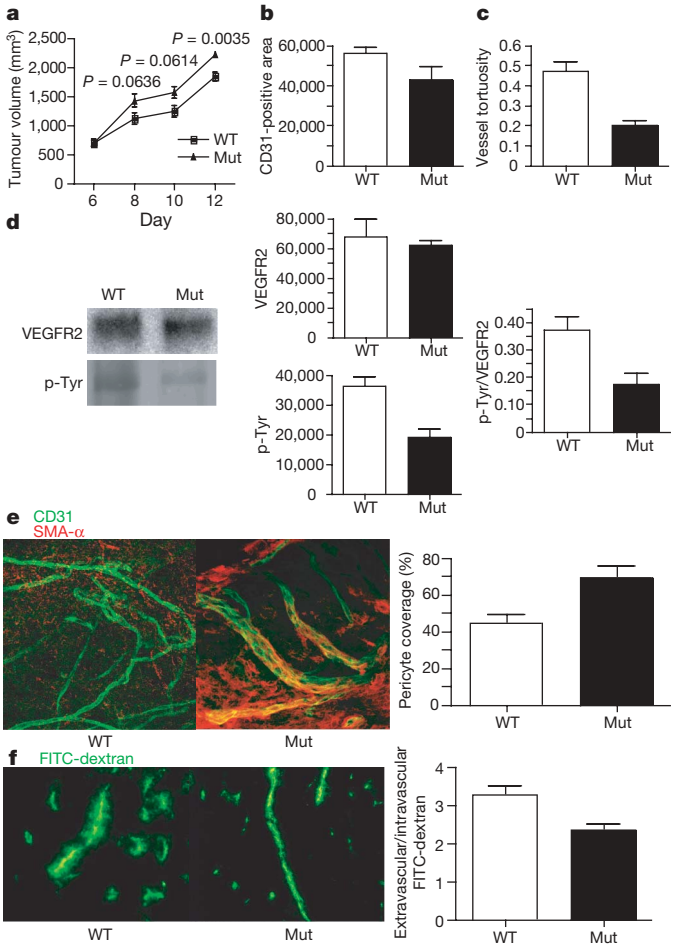

Figure 2 | Deletion of VEGF in myeloid cells leads to a normalized vasculature and higher tumour volumes in LLC. a, Growth-curve analysis of LLC tumours injected subcutaneously into WT and mutant mice ($n > 7$ for each group). **b**, Quantitative analysis of pixels corresponding to CD31-positive endothelial cells ($n = 4$). $P = 0.0406$. **c**, Determination of blood vessel tortuosity in LLC tumours. $P = 0.0022$. **d**, Left: immunoblotting for VEGFR2 and phosphotyrosine (p-Tyr) after immunoprecipitation of VEGFR2 from LLC tumour lysates. Centre: quantitative analysis of VEGFR2 (upper; $P = 0.7460$) and phosphotyrosine (lower; $P = 0.0304$) signals as measured by photon emission. Right: ratio of p-Tyr to VEGFR2 signal intensities as a measure of receptor activation (WT $n = 8$, mutant $n = 7$); $P = 0.0075$. **e**, Left: confocal microscopy images of simultaneous immunodetection of endothelial cells and pericytes in LLC tumours with the specific markers CD31 and smooth muscle actin-α (SMA-α). Right: pericyte coverage as assessed by SMA-α/CD31 co-localization ($n = 4$). $P = 0.0201$. **f**, Left: fluorescent microscopy images of fluorescein isothiocyanate (FITC)-dextran angiography on LLC isografts. Right: ratio of extravascular to intravascular FITC-dextran as a measure of vascular permeability (WT $n = 6$, mutant $n = 4$). $P = 0.0217$. Error bars show s.e.m.

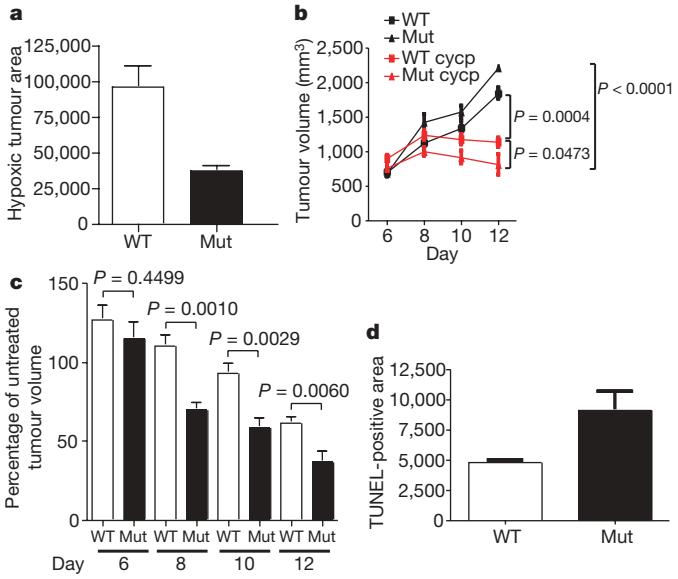

Figure 3 | Deletion of VEGF in myeloid cells results in reduced hypoxia and increased susceptibility of LLC tumours to cytotoxic agents. a, Quantitative analysis of pixels corresponding to hypoxic tumour areas (WT $n = 6$, mutant $n = 4$). $P = 0.0112$. **b**, Growth-curve analysis of LLC isografts from WT and mutant animals ($n > 4$ for each group) treated with cyclophosphamide (cycp; 170 mg kg^{-1}) at days 6, 8 and 10 after tumour implantation. **c**, Response of tumours from WT and mutant mice to treatment with cyclophosphamide, expressed as the percentage of treated tumour volume to untreated tumour volume at the specified time points. **d**, Quantitative analysis of TdT-mediated dUTP nick end labelling (TUNEL) positive area on cyclophosphamide-treated LLC isografts ($n = 4$). $P = 0.0343$. Error bars show s.e.m.

tumour-bearing mice. Loss of myeloid-derived VEGF increased the chemotherapeutic efficacy of the treatment (Fig. 3b, c). The cyclophosphamide treatment also resulted in a significantly increased level of tumour cell death in mice bearing tumours lacking myeloid VEGF-A, as can be seen in Supplementary Fig. 3e and as quantified in Fig. 3d. Similar experiments performed with the cytotoxic drug *cis*-platinum gave comparable results (Supplementary Fig. 3f, g).

To determine the differential contributions of tumour-cell and myeloid-cell-derived VEGF, we next created fibrosarcoma cell lines derived from C57Bl/6J embryos homozygous for the conditional allele of the *Vegfa* gene. We then used Cre recombinase expression from adenovirus to create matching WT (infected with control adenovirus) and *Vegfa*-null (infected with Cre recombinase-expressing adenovirus) tumour cell lines, and injected them subcutaneously into mice that were WT or null for myeloid VEGF-A expression. As can be seen in Fig. 4a, fibrosarcomas that were WT for VEGF-A expression grew faster and significantly larger in mice lacking *Vegfa* in myeloid cells, which is similar to what we observed in the other models described above. However, in agreement with previous findings from our laboratory[8], tumours lacking VEGF-A expression grew more slowly than those expressing VEGF-A, when implanted into WT mice (Fig. 4a).

When VEGF-A was absent from both the tumour and the myeloid compartment, tumour growth essentially collapsed, with greatly increased apoptosis and necrosis (Fig. 4a–f). Further, although there was a decrease in tumour vessel density (Fig. 4b, d) ranging from the highest vessel count in tumours that were WT in all tissue compartments, to the lowest in those lacking VEGF-A in tumour cells and myeloid cells, these values did not correspond directly to changes in tumour growth; rather, they demonstrate the unique role for myeloid-derived VEGF-A in facilitating changes in tumour vessel function and normalization.

Tumour-associated macrophages have been shown to be crucial for malignant progression in a mouse model of breast cancer[7,9]; however, these studies removed macrophages completely from tumours and were therefore removing all of the many aspects of macrophage involvement in tumour progression. In isolating one of those aspects experimentally, we have shown that myeloid-derived VEGF-A is required for the formation of a high-density vessel network, that loss of VEGF-A from this source greatly decreases the activation of VEGFR2 in spite of little or no loss in total tumour VEGF-A, and that the absence of this increased vascular density does not hamper, but rather accelerates, tumour progression.

When administered as single agents, anti-angiogenic drugs have produced modest objective responses in clinical trials, but overall these single-agent approaches have not yielded significant long-term survival benefits[10]. In contrast, when given in combination with chemotherapy, antibodies targeted against VEGF-A result in an increase in survival in colorectal cancer patients[11]. Our observations

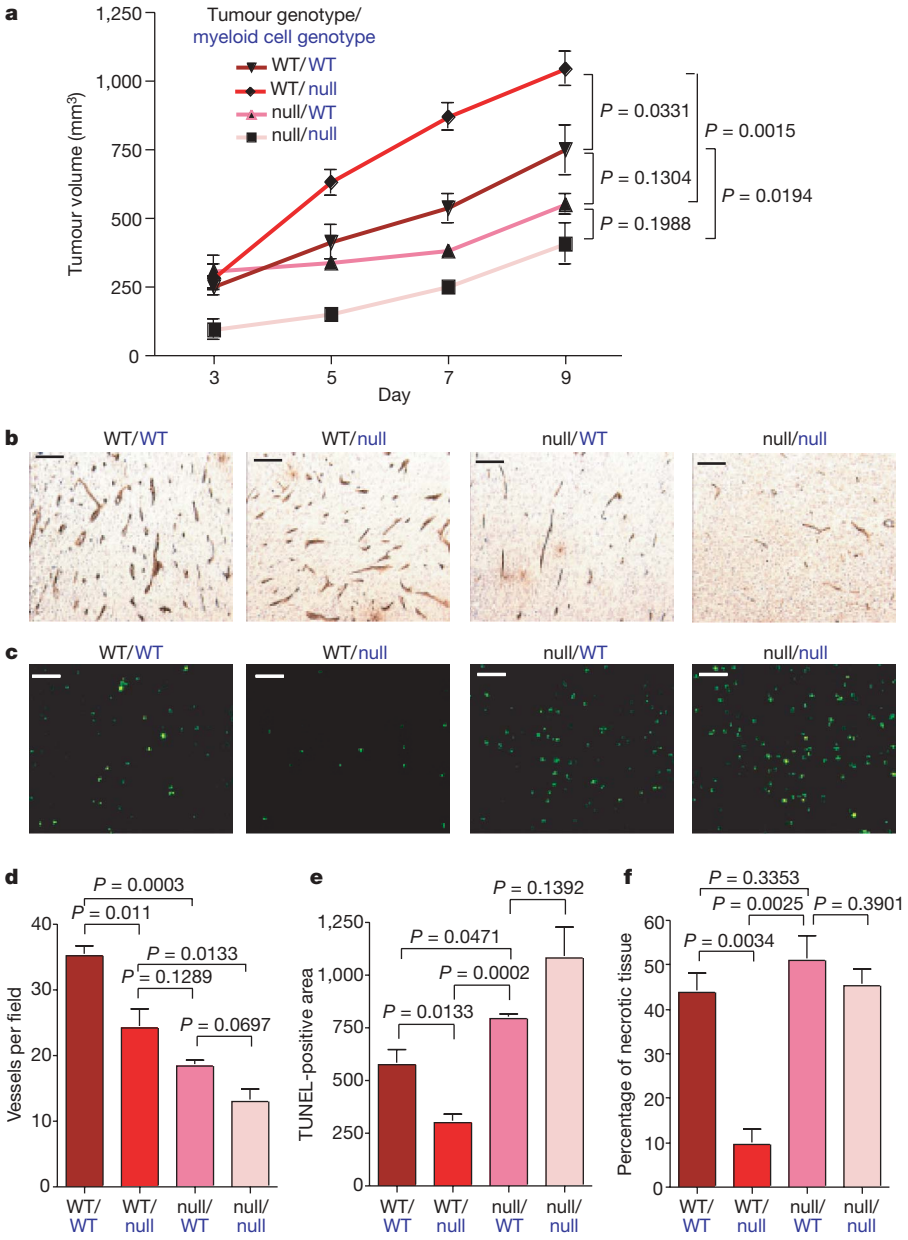

Figure 4 | Effect of tumour-cell-derived versus myeloid-cell-derived VEGF on tumour angiogenesis and growth. **a**, Growth-curve analysis of wild-type (WT) and VEGF nullizygous (null) fibrosarcoma isografts (genotype labelled in black) implanted into WT mice or mutant mice (null) with a myeloid-cell-specific deletion of *VEGF* (genotype labelled in blue) ($n = 4$ for each group). **b**, CD34 immunostaining on fibrosarcoma isografts. **c**, Detection of apoptotic cells in fibrosarcomas by TUNEL staining. **d**, Quantitative analysis of CD34-positive blood vessels ($n = 4$). **e**, Quantification of TUNEL-positive cells ($n = 4$). **f**, Assessment of tumour necrosis on fibrosarcoma midline sections. Shown is the perimeter of necrotic areas expressed as a percentage of the total tumour perimeter ($n = 4$). Scale bars, 100 μm. Error bars show s.e.m.

argue that a critical mediator of this sensitization to chemotherapy lies in the infiltrating innate immune cells rather than in the malignant cells of the tumour. These findings open a new avenue for the investigation of anti-angiogenic therapies targeted to tumour-associated cells of the immune system.

METHODS SUMMARY

Transgenic mice (C57Bl/6J) expressing the polyoma middle T (PyMT) oncoprotein under the promoter of the mouse mammary tumour virus (MMTV) long terminal repeat were bred to mice (C57Bl/6J) with both alleles of exon 3 of *Vegfa* flanked by *loxP* sites (*VEGF*+^{f}/+^{f})[12]. Myeloid cell-specific knockout of VEGF was achieved by breeding male mice homozygous for the floxed *Vegfa* allele and hemizygous for the PyMT oncogene (MMTV-*PyMT*/*VEGF*+^{f}/+^{f}) with female mice (C57Bl/6J) homozygous for the floxed *Vegfa* allele expressing Cre recombinase driven by the lysozyme M promoter (*LysMCre*+/*VEGF*+^{f}/+^{f})[4]. For our studies, we used female mice hemizygous for the *PyMT* oncogene carrying two floxed *Vegfa* alleles and positive for Cre expression (MMTV-*PyMT*/*LysMCre*+/*VEGF*+^{f}/+^{f}), designated as mutants, whereas female littermates negative for Cre expression (MMTV-*PyMT*/*LysMCre*−/*VEGF*+^{f}/+^{f}) served as WT controls. Loss of VEGF-A expression in myeloid cells had no effect on normal mammary development (Supplementary Fig. 1c).

To generate isografts, 10^7 LLC cells on a BL6 background (ATCC) were injected subcutaneously into *LysMCre*−/*VEGF*+^{f}/+^{f} (WT) and *LysMCre*+/*VEGF*+^{f}/+^{f} mice (mutant). Mouse embryonic fibroblasts (MEFs) were isolated from WT mice. The transgenic MEFs were immortalized by stable transfection with SV40 large T antigen and then transformed with a vector expressing oncogenic mutant H-Ras (Val 12). Subsequently, the *VEGF*+^{f}/+^{f} MEFs were infected with an adenovirus expressing Cre recombinase to delete exon 3 of the *Vegfa* gene. A total of 5×10^6 VEGF-A-null or WT MEFs were injected subcutaneously into WT and mutant mice. Data are expressed as means ± s.e.m. Statistical significance was determined by a two-tailed unpaired *t*-test.

Full Methods and any associated references are available in the online version of the paper at www.nature.com/nature.

Received 29 March; accepted 12 September 2008.
Published online 9 November 2008.

1. Folkman, J. Angiogenesis. *Annu. Rev. Med.* **57,** 1–18 (2006).
2. Lewis, J. S., Landers, R. J., Underwood, J. C., Harris, A. L. & Lewis, C. E. Expression of vascular endothelial growth factor by macrophages is up-regulated in poorly vascularized areas of breast carcinomas. *J. Pathol.* **192,** 150–158 (2000).
3. Gerber, H. *et al.* VEGF couples hypertrophic cartilage remodeling, ossification and angiogenesis during endochondral bone formation. *Nature Med.* **5,** 623–628 (1999).
4. Clausen, B. E., Burkhardt, C., Reith, W., Renkawitz, R. & Forster, I. Conditional gene targeting in macrophages and granulocytes using LysMcre mice. *Transgenic Res.* **8,** 265–277 (1999).
5. Cramer, T. *et al.* HIF-1α is essential for myeloid cell-mediated inflammation. *Cell* **112,** 645–657 (2003).
6. Guy, C. T., Cardiff, R. D. & Muller, W. J. Induction of mammary tumors by expression of polyomavirus middle T oncogene: a transgenic mouse model for metastatic disease. *Mol. Cell. Biol.* **12,** 954–961 (1992).
7. Lin, E. Y. *et al.* Progression to malignancy in the polyoma middle T oncoprotein mouse breast cancer model provides a reliable model for human diseases. *Am. J. Pathol.* **163,** 2113–2126 (2003).
8. Grunstein, J., Roberts, W. G., Mathieu-Costello, O., Hanahan, D. & Johnson, R. S. Tumor-derived expression of vascular endothelial growth factor is a critical factor in tumor expansion and vascular function. *Cancer Res.* **59,** 1592–1598 (1999).
9. Lin, E. Y. *et al.* Macrophages regulate the angiogenic switch in a mouse model of breast cancer. *Cancer Res.* **66,** 11238–11246 (2006).
10. Mayer, E. L., Lin, N. U. & Burstein, H. J. Novel approaches to advanced breast cancer: bevacizumab and lapatinib. *J. Natl. Compr. Canc. Netw.* **5,** 314–323 (2007).
11. Hurwitz, H. I., Honeycutt, W., Haley, S. & Favaro, J. Long-term treatment with bevacizumab for patients with metastatic colorectal cancer: case report. *Clin. Colorectal Cancer* **6,** 66–69 (2006).
12. Gerber, H. P. *et al.* VEGF is required for growth and survival in neonatal mice. *Development* **126,** 1149–1159 (1999).

Supplementary Information is linked to the online version of the paper at www.nature.com/nature.

Acknowledgements We thank J. DuRose, N. Ferrara, L. Iruela-Arispe, L. Coussens, M. Karin, V. Nizet and H.-P. Gerber for helpful conversations. Financial support was provided by the Deutsche Forschungsgemeinschaft to C.S. (STO 787/1-1) and A.W. (WE 4275/1-1), a Susan G. Komen Dissertation Research Award (DISS0402406) to A.D., and National Institutes of Health grants CA82515, CA118165 and AI060840 to R.S.J.

Author Contributions C.S. generated isografts, conducted drug treatment studies, performed biochemical experiments, immunohistochemical procedures and histological analysis, and prepared the manuscript. A.D. generated MMTV-*PyMT/LysMCre/VEGF*+^{f}/+^{f} mice, conducted related tumour palpation/mass studies, initial histology and flow cytometry, and assisted with the manuscript. A.W. generated VEGF-null fibroblasts. N.Z. performed preliminary cDNA studies on MMTV-*PyMT/LysMCre/VEGF*+^{f}/+^{f} tumours. N.T. assisted with the fluorescein isothiocyanate-dextran angiography. J.I.G. and D.A.C. provided confocal microscopy images and technical advice. R.S.J. supervised and directed the project.

Author Information Reprints and permissions information is available at www.nature.com/reprints. Correspondence and requests for materials should be addressed to R.S.J. (rsjohnson@ucsd.edu).

METHODS

Chemotherapy. The treatment with chemotherapy was started six days after injection of 10^7 LLC cells. Cisplatin (5 mg kg^{-1}) and cyclophosphamide (170 mg kg^{-1}) were purchased from Sigma and given intraperitoneally on alternate days until day 10.

Histology, immunohistochemistry and immunofluorescence. For whole-mount preparation of mammary glands, the inguinal gland was removed and fixed in 10% phosphate-buffered formalin (Fisher Scientific) and dehydrated through a series of graded acetone and ethanol washes. Glands were stained for 3 h with Harris haematoxylin (VWR International), and excess stain was removed by washing in water. Glands were destained in acidic 50% ethanol and dehydrated and stored in methyl salicylate (Fisher Scientific).

After removal, tumours were fixed in 10% formalin, zinc fixative (BD Pharmingen) or 4% paraformaldehyde, respectively, and then embedded in paraffin. For haematoxylin/eosin staining and immunostaining, 5-μm sections were deparaffinized with xylene and rehydrated with graded ethanol. The sections were stained in accordance with routine immunohistochemistry procedures and revealed with Vectastain ABC or ABC-AP kit (Vector Laboratories).

Primary antibodies used for immmunohistochemistry and immunofluorescence. Biotinylated rat anti-CD31 at 1:100 dilution (BD Pharmingen), rat anti-CD34 (Novus), biotinylated mouse anti-PCNA at 1:800 dilution (BD Pharmingen), biotinylated rat anti-F4/80 at 1:200 dilution (Serotec), rabbit anti-VEGF at 1:50 dilution (sc-152; Santa Cruz) and mouse anti-SMA-α at 1:500 dilution (Chemicon) were used. Fluorochrome-conjugated Alexa 488 and Alexa 555 were used as secondary antibodies (1:200 dilution).

Pimonidazole hydrochloride (Hypoxyprobe-1) was injected intraperitoneally (60 mg kg^{-1} body weight) 1 h before tumour removal and was detected with a Mouse IgG_1 monoclonal antibody (Mab1; Natural Pharmacia International).

TUNEL assay (Promega) was performed in accordance with the manufacturer's instructions.

Quantitative analysis of histological markers. For quantitative analysis of the distribution of immunohistochemical markers within the tumour, the midline sections of tumours were photographed into TIFF images with a Leica DMR microscope and SPOT RT colour camera system (Diagnostic Instruments Inc.) and the area (number of pixels) with positive staining equal to or greater than a set threshold was measured with the Image J program; such marked areas were normalized by the number of images for each tumour. For comparison at different stages of progression, PyMT tumours were classified as described previously[7].

To determine vessel density, the vasculature marked by CD31 and CD34 was skeletonized with the Image J program; the area covered by blood vessels was measured and the number of vessels per field was determined, respectively.

To estimate change in vessel length, the skeletonized blood vessels that showed up in a longitudinal cut within an image were traced along their midline and the number of pixels was converted into distance in millimetres with Image J.

The tortuosity (T) of blood vessel is defined as $T = L/S - 1$, where L is the length of the vessel of interest and S is the straight-line distance between its endpoints.

Confocal microscopy. Co-localization of pericytes (SMA-α) endothelial cells (CD31) was imaged on 20-μm sections of excised LLC tumours. Images were acquired with laser-scanning confocal microscopy under a 60×/1.4 numerical aperture oil-immersion objective (Nikon C1si; Nikon Instruments Inc.).

Flow cytometry. Tumours were excised and cut into small pieces before incubation in a shaker at 37 °C at 250 r.p.m. for 2 h in 0.1% collagenase A (Roche) in RPMI 1640 medium (Invitrogen). The resulting single-cell suspension was pelleted and rinsed in PBS before treatment with hypotonic lysis buffer and passing through a 40-μm cell strainer (BD Biosciences). For each condition, 10^6 cells were then incubated with Fc Block (BD Biosciences) to block non-specific FcR binding before labelling with fluorescently conjugated antibodies (eBiosciences) with standard protocols. Data were acquired on a FACSCalibur flow cytometer (BD Biosciences) with propidium iodide to exclude non-viable cells, and analysed with FlowJo software (Tree Star).

Determination of vascular permeability. FITC-dextran (200 μl; 2 MDa; Sigma) were injected intravenously at a concentration of 50 mg ml^{-1}. After 10 min, tumours were removed and immediately frozen in OCT compound. Cryosections 10 μm thick were cut, and vascular permeability was determined on the basis of ten randomly taken pictures from each tumour. With the use of Image J the edges of blood vessels were indentified and the extravascular and intravascular areas (numbers of pixels) covered by FITC-dextran were measured. To determine vascular permeability in a quantitative manner, the ratio of extravascular staining to intravascular FITC-dextran was calculated.

Immunoprecipitation and immunoblotting. Tumours were lysed in RIPA buffer and 500 μg of lysate was used for immunoprecipitation of VEGFR2. The following antibodies were used in this study: rabbit anti-VEGFR2 (55B11; Cell Signaling), horseradish peroxidase-conjugated anti-phosphotyrosine (4G10; Millipore), rabbit anti-VEGF (sc-152; Santa Cruz) and mouse anti-β-actin (Sigma). For quantitative analysis the membranes were scanned with a fluorescence scanner and the signal strength was determined with ImageQuant software.

Determination of deletion frequency and gene expression by quantitative PCR. Thioglycollate-elicited macrophages as well as FACS-sorted F4/80-positive tumour-associated macrophages isolated from PyMT-mutant tumours were used for isolation of genomic DNA as described previously[5]. Whole tumours were ground to a fine powder in liquid nitrogen and subsequently homogenized in TRIzol reagent (Invitrogen). Total RNA was isolated in accordance with the manufacturer's instructions. For real-time PCR analysis, the isolated RNA was reverse transcribed. For PCR reactions, TaqMan-Universal Mastermix (Applied Biosytems) was used. cDNA (50 ng) was used as template to determine the relative amount of mRNA by real-time PCR (ABI Prism 7700 sequence detection system), using specific primers and probes with the following sequences: VEGF, 5′-ATCCGCATGATCTGCATGG-3′ (reverse), and 5′-AGTCCCATGAAGTGATCAAGTTCA-3′ (forward); VEGF probe, (6FAM)TGCCCACGTCAGAGAGCAACATCAC(BHQ-1); PGK, 5′-TTCTTGCTGCTCTCAGTACCACA-3′ (reverse) and 5′-CAAATTTGATGAGAATGCCAAGACT-3′ (forward); PGK probe, (6FAM)TATACCTGCTGGCTGGATGGGCTTGGACT(BHQ-1) (6FAM is 6-carboxyfluorescein; BHQ-1 is Black hole quencher (ABI)).

Cell culture. Cells were cultured in DMEM High Glucose medium, supplemented with 10% fetal bovine serum, 2 mM glutamine, 50 U ml^{-1} penicillin and 100 μg ml^{-1} streptomycin.